Geochemistry Geophysics Geosystems G3

Published by AGU and the Geochemical Society

Article
Volume 14, Number 2
4 February 2013
doi:10.1029/2012GC004429
ISSN: 1525-2027

Oligocene-Miocene magnetic stratigraphy carried by biogenic magnetite at sites U1334 and U1335 (equatorial Pacific Ocean)

J. E. T. Channell
Department of Geological Sciences, University of Florida, P.O. Box 112120, Gainesville, Florida, 32611, USA (jetc@ufl.edu)

C. Ohneiser
Department of Geology, University of Otago, Dunedin, New Zealand

Y. Yamamoto
Center for Advanced Marine Core Research, Kochi University, Nankoku, Kochi, Japan

M. S. Kesler
Major Analytical Instrumentation Center (MAIC), University of Florida, Gainesville, Florida, USA

[1] Sediments from the equatorial Pacific Ocean, at the Integrated Ocean Drilling Program sites U1334 and U1335, record reliable magnetic polarity stratigraphies back to ~26.5 Ma (late Oligocene) at sedimentation rates usually in the 5–20 m/Myr range. Putative polarity subchrons that do not appear in current polarity timescales occur within Chrons C5ACr, C5ADn, and C5Bn.1r at Site U1335; and within Chrons C6AAr.2r, C6Br, C7Ar, and C8n.1n at Site U1334. Subchron C5Dr.1n (~17.5 Ma) is recorded at both sites, supporting its apparent recording in the South Atlantic Ocean, and has an estimated duration of ~40 kyr. The Oligocene-Miocene calcareous oozes have magnetizations carried by submicron magnetite, as indicated by thermal demagnetization of magnetic remanences, the anhysteretic remanence to susceptibility ratio, and magnetic hysteresis parameters. Transmission electron microscopy of magnetic separates indicates the presence of low-titanium iron oxide (magnetite) grains with size (50–100 nm) and shape similar to modern and fossil bacterial magnetite, supporting other evidence that biogenic submicron magnetite is the principal remanence carrier in these sediments. In the equatorial Pacific Ocean, low organic-carbon burial arrests microbial pore-water sulfate reduction, thereby aiding preservation of bacterial magnetite.

Components: 7,900 words, 13 figures, 2 tables.

Keywords: magnetic stratigraphy; equatorial Pacific; Oligocene-Miocene; biogenic magnetite.

Index Terms: 1520 Magnetostratigraphy: Magnetostratigraphy; 1535 Magnetostratigraphy: Reversals: process, timescale, magnetostratigraphy; 1505 Magnetostratigraphy: Biogenic magnetic minerals.

Received 10 September 2012; **Revised** 7 November 2012; **Accepted** 15 November 2012; **Published** 4 February 2013.

Channell, J. E. T., C. Ohneiser, Y. Yamamoto, and M. S. Kesler (2012), Oligocene-Miocene magnetic stratigraphy carried by biogenic magnetite at sites U1334 and U1335 (equatorial Pacific Ocean), *Geochem. Geophys. Geosyst.*, *14*, 265–282, doi:10.1029/2012GC004429.

1. Introduction

[2] Oligocene-Miocene sediments from the equatorial Pacific Ocean have played an important role in the generation of the geomagnetic polarity timescale (GPTS), and hence geologic timescales. In the early 1970s, sediments from this region provided the first Miocene polarity stratigraphies [e.g., *Opdyke et al*., 1974; *Theyer and Hammond*, 1974] for comparison with emerging marine magnetic anomaly records [e.g., *Blakely*, 1974; *Klitgord et al*., 1975]. More recently, the Ocean Drilling Program Legs 138 and 199 in 1991 and 2001, respectively, provided important reference records for Oligocene-Miocene magnetic polarity stratigraphy [e.g., *Schneider*, 1995; *Pares and Lanci*, 2004; *Lanci et al*., 2004, 2005] that led to improvements in geologic timescales by tying astronomically calibrated cyclostratigraphies to polarity chrons [*Shackleton et al*., 1995; *Pälike et al*., 2006]. Polarity chron interpretations in the Miocene are, however, problematic at pelagic sedimentation rates because of high reversal frequency. As a result, there are few Miocene magnetic stratigraphies in which the polarity chron interpretation is unequivocal. Magnetic stratigraphies from the equatorial Pacific Ocean presented here provide some of the higher quality Miocene magnetic stratigraphies available, and contribute to the effort to provide interpretable late Oligocene-Miocene polarity records for correlation with bio-, chemo-, and cyclostratigraphies.

[3] Here we report on the magnetic polarity stratigraphy from two sites (sites U1334 and U1335) drilled from the R/V *Joides Resolution* during the Integrated Ocean Drilling Program (ODP) Expeditions 320 and 321 [*Pälike et al*., 2010, 2012] that were part of a single drilling program designed to core sediments along a Pacific Equatorial Age Transect (Figure 1). Each site was selected to recover a portion of the interval spanning the early Eocene through Pleistocene, which complements the Paleocene/Eocene and late Miocene to recent intervals recovered by previous paleoequatorial Pacific Ocean drilling during ODP Legs 138 and 199 [e.g., *Shackleton et al*., 1995; *Pälike et al*., 2006]. A principal objective of Expedition 320/321 was to improve and extend the astronomical calibration of the geological timescale for the Cenozoic by integrating orbitally forced variations in the sediment composition with bio-, chemo-, and magnetostratigraphic records, and to place the Cenozoic paleoceanography of the equatorial Pacific Ocean into this refined temporal framework.

2. Samples and Methods

[4] Shipboard magnetic measurement of the natural remanent magnetization (NRM) and volume susceptibility were carried out on split half-core sections. The NRM of sites U1334 and U1335 was measured shipboard, usually at 5 cm intervals, prior to demagnetization, and then after demagnetization at peak fields of 20 mT [*Expedition 320/321 Scientists*, 2010a, 2010b]. Postcruise measurements were carried out on u-channel samples, which are $2 \times 2 \times 150$ cm samples encased in plastic with a clip-on lid that constitutes one of the sides, collected from archive-halves of the composite splice assembled from separate holes drilled at the site [see *Expedition 320/321 Scientists*, 2010a, 2010b]. The u-channels were collected in the 0–160 meters composite depth (mcd) interval (~0–26.5 Ma) at Site U1334, and the 123–227 mcd interval (~13–18.5 Ma) at Site U1335. The intervals for u-channel sampling were dictated by results from shipboard investigations. At Site U1334, an abrupt change in sediment color from light tan to greenish gray occurs at ~160 mcd, as denoted by a decrease in a* (green-red) and b* (blue-yellow) reflectance parameters (see *Expedition 320/321 Scientists* [2010a, Figure F32]). The color change is accompanied by a sharp decrease in susceptibility and NRM intensity to levels below instrument noise. The greenish-gray interval at Site U1334 extends to ~230 mcd, which coincides with the base of the advanced piston core section. At Site U1335, the u-channel sampled interval (123–227 mcd) coincides with an early-middle Miocene interval where shipboard magnetic records indicated a relatively high fidelity paleomagnetic record at elevated sedimentation rates, and numerous putative subchrons that do not appear in current versions of the GPTS.

[5] The NRM of u-channel samples was measured using a track designed for u-channel samples, aligned with an alternating field demagnetization system and a 2G Enterprises cryogenic magnetometer, located at the University of Florida [see *Weeks et al*., 1993; *Guyodo et al*., 2002]. The NRM was measured at 1 cm intervals with a 10 cm leader and trailer at the ends of the u-channel sample, using tracking speeds of 10 cm/s. After initial NRM measurement, samples were measured after each stepwise demagnetization step in 2.5 mT increments in the 20–40 mT peak-field range, 5 mT increments in the 40–50 mT range, and 10 mT increments in the 50–80 mT interval. The detailed demagnetization protocol was designed to facilitate definition of magnetization components using

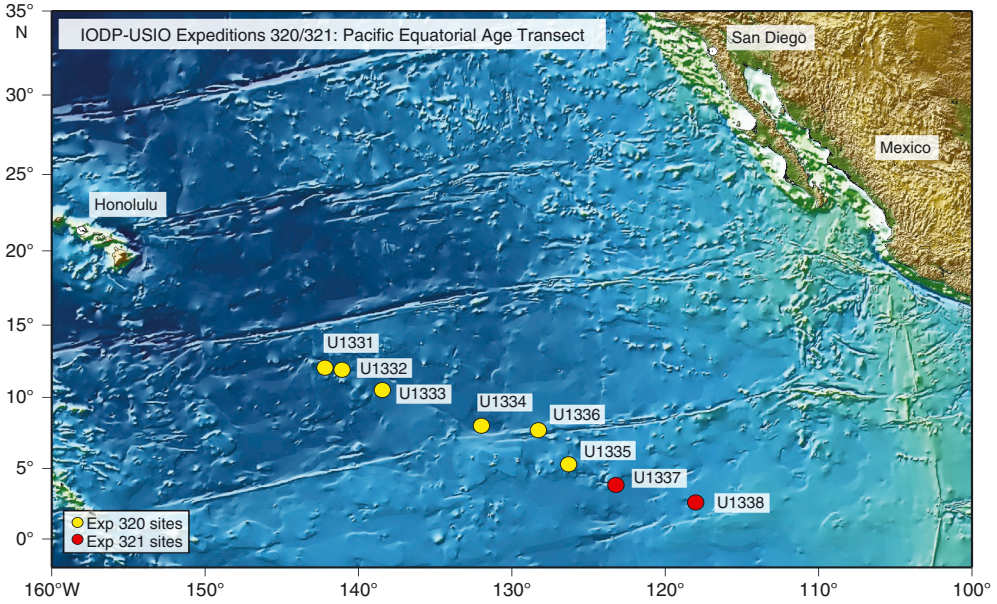

Figure 1. Location map for sites drilled during IODP Expedition 320/321.

standard principal component analysis [*Kirschvink*, 1980a] method as implemented in the MATlab program, UPmag [*Xuan and Channell*, 2009]. The maximum angular deviation (MAD) of each principal component value monitors the quality of magnetization components, computed at 1 cm intervals.

[6] After measurement of the NRM, volume susceptibility was measured using a susceptibility track designed for u-channel samples [*Thomas et al.*, 2003]. This was followed by acquisition of an anhysteretic remanent magnetization (ARM) in an alternating field of 100 mT with a 39.79 A/m (50 μT) DC bias field. The ARM was demagnetized up to a peak field of 60 mT in the same field increments as for the NRM. The ratio of ARM intensity to susceptibility can be used as a means of estimating the grain size of magnetite [see *King et al.*, 1983] because ARM intensity is more sensitive to the concentration of fine-grained (submicron) magnetite, whereas susceptibility has enhanced sensitivity to coarser (tens of microns) magnetite.

[7] Additional mineralogical information was acquired using magnetic hysteresis data measured on a Princeton Measurements Corporation vibrating sample magnetometer. Hysteresis ratios (M_r/M_s and H_{cr}/H_c where M_r is saturation remanence, M_s is saturation magnetization, H_{cr} is coercivity of remanence, and H_c is coercive force) can be used to delineate single domain (SD), pseudosingle domain (PSD), and multidomain (MD) magnetite and to assign "mean" magnetite grain sizes through empirical and theoretical calibrations of the so-called Day plot [*Day et al.*, 1977; *Carter-Stiglitz et al.*, 2001; *Dunlop*, 2002a, 2002b; *Dunlop and Carter-Stiglitz*, 2006]. Magnetic hysteresis properties were also analyzed using first-order reversal curves (FORC diagrams) that provide enhanced mineral and domain state discrimination [*Pike et al.*, 1999; *Roberts et al.*, 2000; *Muxworthy and Roberts*, 2007]. FORCs were measured by progressively saturating a small (few hundred mg) sample in a field (H_{sat}), decreasing the field to a value H_a, reversing the field and sweeping it back to H_{sat} in a series of regular field steps (H_b). The process is repeated for many values of H_a. The magnetization is then represented as a contour plot with axes H_c and H_u where $H_c = (H_b - H_a)/2$ and $H_u = (H_b + H_a)/2$. The contoured distribution of a FORC diagram can be interpreted in terms of the coercivity distribution along the H_c axis. Spreading of the distribution along the H_u axis is indicative of magnetostatic interactions for SD grains or internal demagnetizing fields for MD grains. In general, closed peaked structures along the H_c axis are characteristic of SD grains, with contours becoming progressively more parallel to the H_u axis with grain size coarsening [*Pike et al.*, 1999]. FORC diagrams were analyzed using the software of *Harrison and Feinberg* [2008] with a smoothing factor of 6. The relatively high smoothing factor value is necessary to suppress noise for the relatively weakly magnetized bulk sediments, in spite of a FORC protocol lasting 3.6 h with an averaging time of 1 s and a field increment of 2 mT up to a maximum applied field of 1 T.

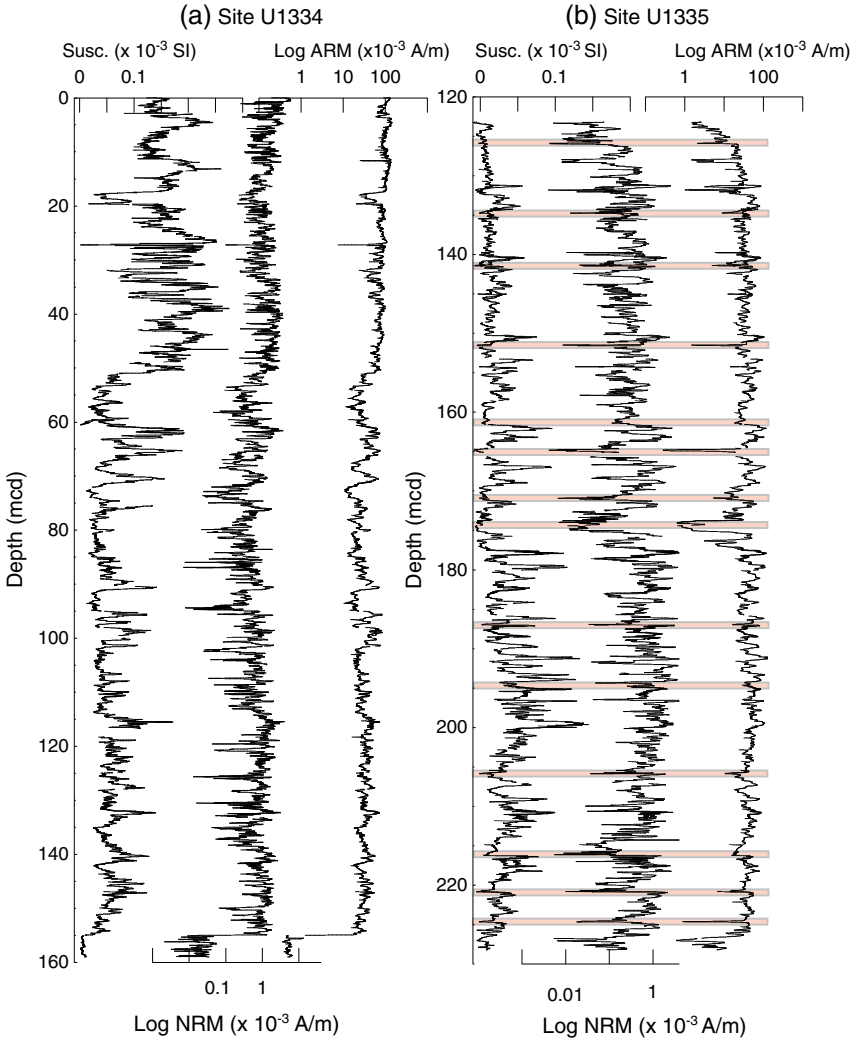

Figure 2. Volume susceptibility, NRM intensity and ARM intensity for (a) Site U1334 and (b) Site U1335. Shading for Site U1335 indicates the location of centimeter- to decimeter-scale beds with sharp basal contacts, interpreted shipboard as gravity flow deposits [see *Expedition 320/321 Scientists*, 2010b, Table T3].

[8] Discrete cubic ($7\,cm^3$) samples from Site U1334 were thermally demagnetized to determine the unblocking temperature spectra of the NRM. In addition, thermal demagnetization of a 3-axis isothermal remanent magnetization (IRM), applied to three mutually orthogonal sample axes for cubic ($7\,cm^3$) samples using DC fields of 0.1, 0.3, and 5 T [*Lowrie*, 1990], was used as an additional means of determining magnetic mineralogy.

3. Magnetic Stratigraphy

[9] Volume magnetic susceptibility at both sites is positive but weak, varying around 5×10^{-5} SI, apart from the uppermost ~50 m at Site U1334 where susceptibilities are several orders of magnitude higher, which reflects the increased clay content in this interval (Figure 2). The uppermost 50 m at Site U1334 comprises clay and radiolarian clay with nannofossil/radiolarian oozes (Lithologic Unit I), whereas nannofossil oozes dominate below this level (Lithologic Unit II) [see *Expedition 320/321 Scientists*, 2010a]. The decrease in susceptibility at ~50 mcd is manifest in NRM and ARM intensity (Figure 2). NRM intensities at both sites are generally in the 10^{-3}–10^{-4} A/m range, about one order of magnitude above the noise level of u-channel magnetometers. ARM intensities are almost two orders of magnitude higher than NRM intensities (Figure 2). At Site U1335, centimeter- to decimeter-scale beds with sharp basal contacts, which were interpreted shipboard as gravity flow deposits [see *Expedition 320/321 Scientists*, 2010b, Table T3], appear as NRM and/or ARM minima

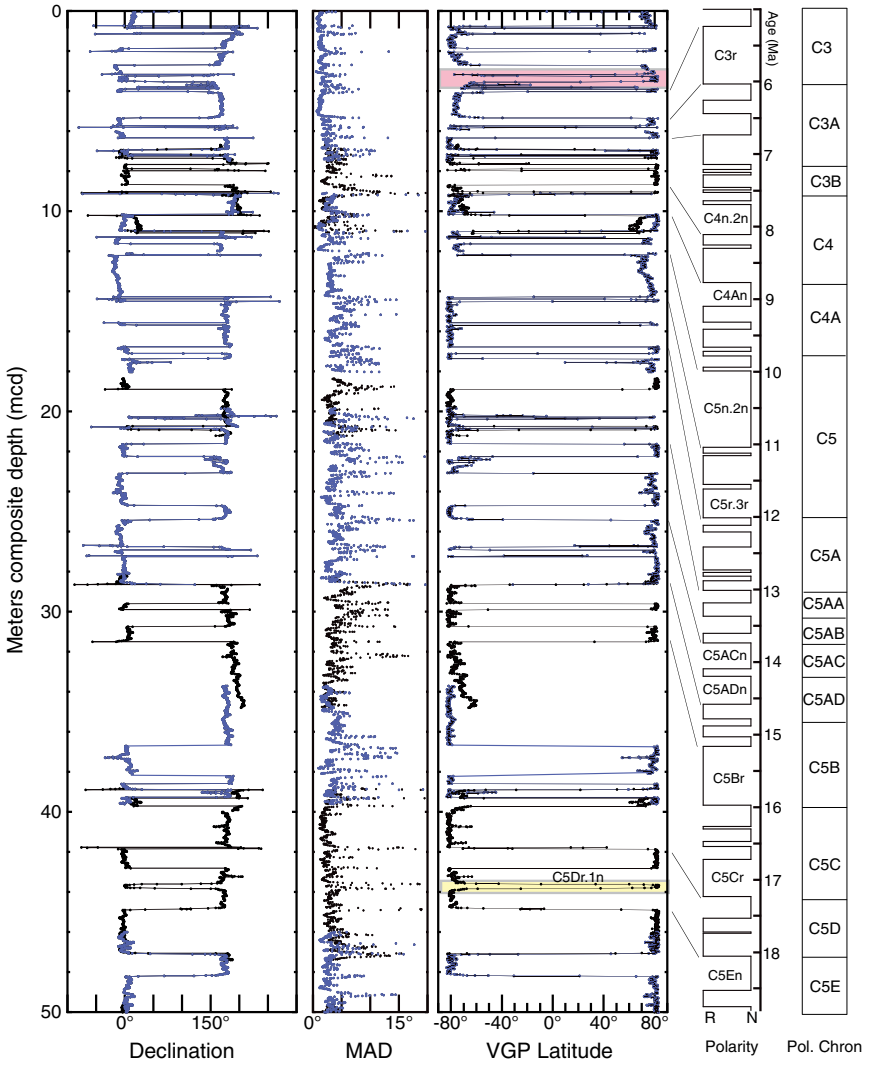

Figure 3. Site U1334: Characteristic component declination, MAD values and VGP latitudes for the 0–50 mcd interval. Components are calculated for a uniform 20–60 mT peak field demagnetization interval. Rarely recorded subchron C5Dr.1n is shaded in yellow. Red shading: magnetostratigraphically undifferentiated Pliocene interval. Alternate holes are color-coded in blue/black.

(shaded in Figure 2b). At 155 mcd at Site U1334, close to the base of the sampled section, susceptibility, NRM intensity, and ARM intensity decrease abruptly coincident with a color change from light tan above to greenish-gray below (Figure 2a).

[10] We calculated magnetization component directions for the 20–60 mT peak field demagnetization interval at the two sites (Figures 3–5). MAD values for this demagnetization interval provide straightforward monitoring of data quality, although, MAD values could be reduced by picking individual demagnetization intervals. This would, however, be a time-consuming task for ~19,000 (12,000) component directions determined each 1 cm downcore at Site U1334 (Site U1335). At both sites, component inclination values are uniformly low due to the location of the sites close to the paleoequator, and therefore are not diagnostic of magnetic polarity. Polarity designations are dependent on component declination. However, cores at sites U1334 and U1335 were, unfortunately, not azimuthally oriented during recovery. Our strategy for orienting cores is critical to interpretation of the magnetic polarity. We first assumed consistent core orientation within each core (no severe core twisting) although minor core twisting is apparent from the declination records of some cores. Second, we rely on consistent declination in overlapping segments of adjacent cores. Finally, we seek to minimize abrupt sedimentation rate changes based on comparison with the

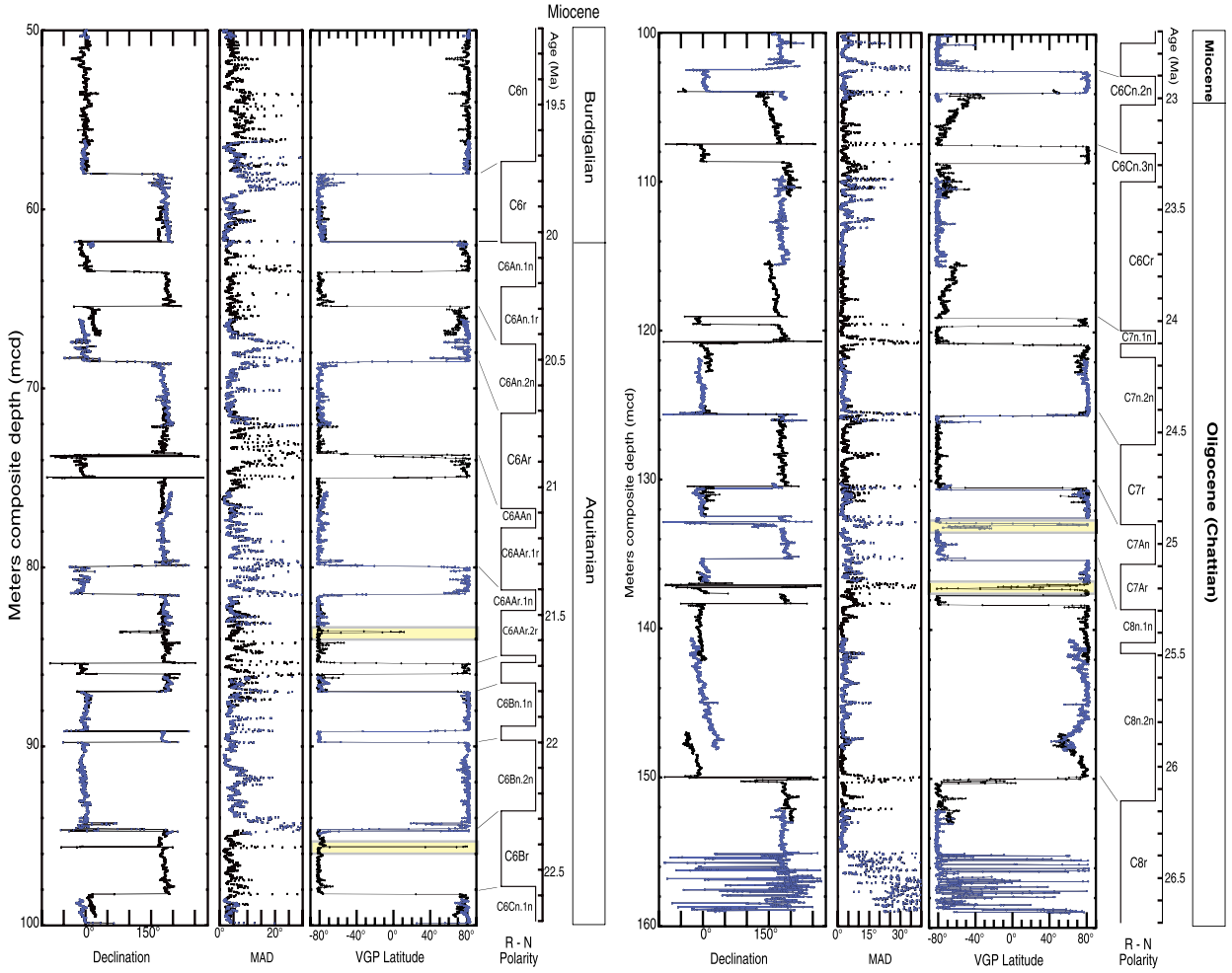

Figure 4. Site U1334: Characteristic component declination, MAD values, and VGP latitudes for Site U1334 (50–100 and 100–160 mcd). Components were calculated for a uniform 20–60 mT peak field demagnetization interval. Putative subchrons, not included in current polarity timescales but apparently recorded within Chrons C6AAr.2r, C6Br, C7Ar, and C8n.1n, are shaded in yellow. Alternate holes are color-coded in blue/black.

GPTS. Using these criteria, in this order, we set mean core declinations to North or South, and then calculated virtual geomagnetic pole (VGP) latitudes, thereby combining inclination and declination data, and we base our polarity interpretations on observed changes in VGP latitude (Figures 3–5).

[11] Our interpretation is greatly dependent on overlapping segments between adjacent cores/holes. Sampling of the optimized composite splice section involves jumps from hole-to-hole at each site [see *Expedition 320/321 Scientists*, 2010a, 2010b]. Alternate holes in the sampled splice are color-coded (blue/black) in Figures 3–5, and one case of appended cores from a single hole is marked (Core 1335B-16H to 1335B-17H at 165 mcd) in Figure 5. We use the *Lourens et al*. [2004] GPTS, extended into the Oligocene by *Ogg and Smith* [2004], as the reference GPTS on the right-hand side of Figures 3–5.

[12] Sedimentation rates were estimated (Figure 6) by comparing three contemporary GPTSs: (1) the Neogene GPTS of *Lourens et al*. [2004] extended into the Oligocene by *Ogg and Smith* [2004]; (2) the GPTS of *Billups et al*. [2004] for the 15–25 Ma interval; and (3) the GPTS of *Pälike et al*. [2006], also for the 15–25 Ma interval. The GPTS of *Pälike et al*. [2006], which is based on magnetostratigraphic and cyclostratigraphic data from the equatorial Pacific Ocean (ODP Site 1218), is similar to that of *Billups et al*. [2004] based on magnetostratigraphic

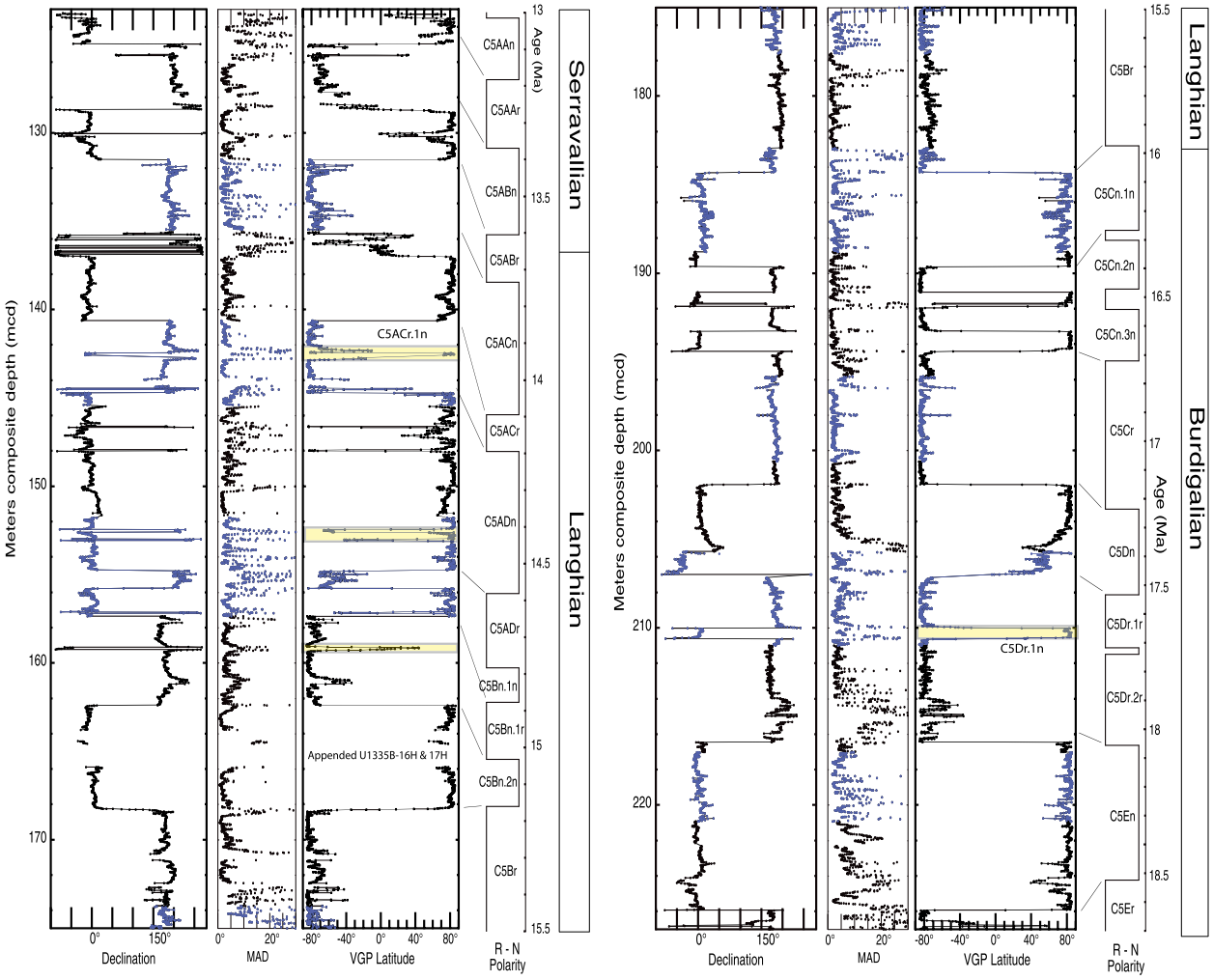

Figure 5. Site U1335: Characteristic component declination, MAD values and VGP latitudes for 123–227 mcd. Components were calculated for a uniform 20–60 mT peak field demagnetization interval. Rarely-recorded subchrons C5ACr.1n and C5Dr.1n, and putative subchrons within C5ADn and C5Bn.1r, are shaded in yellow. Alternate holes are color-coded in blue/black.

and cyclostratigraphic data from the South Atlantic Ocean (ODP Site 1090), but both differ from the GPTS of *Lourens et al.* [2004].

[13] At Site U1334, the uppermost ~17 m (<12 Ma) have low mean sedimentation rates (<3 m/Myr, Figure 6a). The 2–5 Ma interval (the entire Pliocene) at Site U1334 cannot be magnetostratigraphically differentiated (red shading in Figure 3), and has a mean sedimentation rate of ~0.3 m/Myr (Figure 6a). Apart from the uncertainty in this interval, almost all polarity chrons/subchrons featured in the GPTS [e.g., *Lourens et al.*, 2004; *Ogg and Smith*, 2004] are recognized as polarity zones at Site U1334 (Figures 3 and 4, Table 1). The polarity stratigraphy of the entire Miocene and late Oligocene back to Chron C8r at (~26.5 Ma) is readily interpretable at Site U1334. Sedimentation rates are higher (~10–20 m/Myr) in the Late Oligocene and Early Miocene (21–26 Ma) with decreases in sedimentation rate through the Miocene, with the late Miocene (11.6–5.3 Ma) having sedimentation rates of ~2 m/Myr (Figure 6a). A normal polarity subchron within C5Dr (labeled C5Dr.1n and shaded in Figure 3) is identified at Site U1334. This subchron was not included in the *Cande and Kent* [1992, 1995] GPTS, but was identified in South Atlantic magnetic stratigraphy by *Channell et al.* [2003], and subsequently incorporated into the *Lourens et al.* [2004] GPTS. Other possible subchrons recorded at Site U1334 are manifest as thin

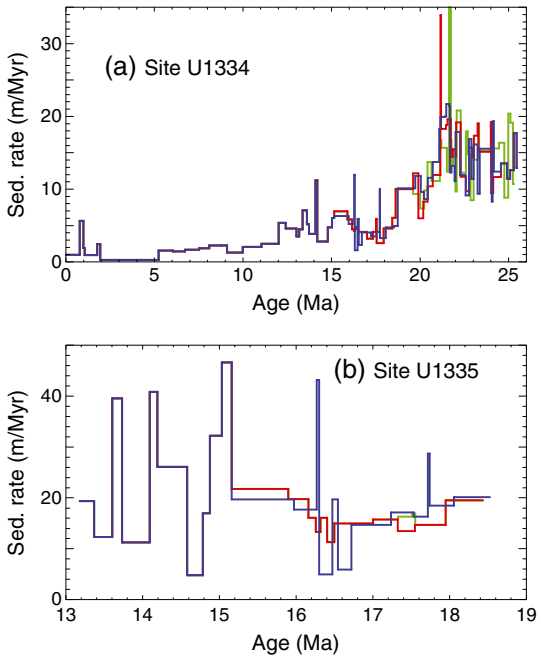

Figure 6. Sedimentation rates for (a) Site U1334 and (b) Site U1335 using the polarity interpretations in Figures 3–5 and the polarity timescales of *Lourens et al.* [2004] (blue line), *Billups et al.* [2004] (red line) and *Pälike et al.* [2006] (green line) where these differ from the *Lourens et al.* [2004] timescale.

normal polarity zones within C6AAr.2r, C6Br, and C7Ar, and a reversed polarity zone within C8n.1n (all shaded in Figure 4). While high MAD values are associated with the boundaries of these putative polarity zones, the polarity zones themselves are all associated with MAD values $<10°$, which implies that they may represent hitherto unrecognized polarity subchrons.

[14] At Site U1335, the polarity interpretation is less straightforward, particularly in the upper part (123–145 mcd), due to apparent reversals at core breaks (Figure 5) and apparent sedimentation rate changes in this depth interval, which corresponds in time to 13–15 Ma (Figure 6b). Our interpretation (Figure 5, Table 2) is largely consistent with the shipboard interpretation for this interval [see *Expedition 320/321 Scientists*, 2010b, Table T20]. A normal polarity subchron within C5ACr (labeled C5ACr.1n and shaded in Figure 5), does not appear in the conventional GPTS, but was apparently identified at ODP Site 1092 [*Evans and Channell*, 2003]. Below 168 mcd (~15.1 Ma) at Site U1335, the polarity interpretation is relatively unequivocal and sedimentation rates are fairly uniform (Figure 6b). Apparent sedimentation rate variations at both sites U1334 and U1335, using the *Lourens et al.* [2004] and *Billups et al.* [2004] timescales, implies inconsistencies in the *Lourens et al.* [2004] GPTS in the vicinity of Chron C5Cn.1r (16.1–16.2 Ma), and perhaps for the three preceding polarity chrons (Figure 6).

[15] As mentioned above, at Site U1335, centimeter- to decimeter-scale beds with sharp basal contacts, which were interpreted shipboard as gravity flow deposits [see *Expedition 320/321 Scientists*, 2010b, Table T3], appear as NRM and/or ARM intensity minima (shaded in Figure 2b). This leads to high MAD values and poor definition of magnetization components over these discrete intervals. We have excluded all component magnetization directions with MAD $> 30°$ in Figure 5, which has eliminated most of the data associated with these gravity flow deposits. We note that Subchron C5Dr.1n is recorded at Site U1335 and Site U1334. In addition, apparent thin polarity zones that do not have analogs in the GPTS, occur within C5ACr, C5ADn (2x), and C5Bn.1r (shaded in Figure 5). Although these polarity zones are associated with some high MAD values at their margins, magnetizations with low MAD values ($<10°$) contribute to their definition.

4. Rock Magnetism

[16] Alternating field (AF) demagnetization of u-channel samples indicates a weak low-coercivity NRM, likely carried by magnetite. Thermal demagnetization of NRM of cubic (7 cm^3) samples from Site U1334 indicates maximum blocking temperatures below 580 °C and dispersed blocking temperature spectra, which are indicative of magnetite (Figure 7). All thermally demagnetized samples have shallow component inclinations apart from one sample (Figure 7, 1334A-4H-6, 85 cm) that lies in a polarity transition (at 39.03 mcd). Component NRM declinations, resolved by thermal demagnetization (Figure 7), are approximately consistent with declination components resolved by AF demagnetization of u-channel samples. For 10 samples collected from different cores at Site U1334, thermal demagnetizations of 3-axis IRMs, where the three IRMs are imposed along the three mutually orthogonal sample axes and acquired sequentially in DC fields of 5 T, 0.3 T, and 0.1 T [*Lowrie*, 1990], indicate a dominant low coercivity (soft) component that acquires an IRM in DC fields <0.1 T, and has maximum blocking temperatures below 580 °C (Figure 8).

Table 1. Depths of Onset of Polarity Chrons Recorded at Site U1334, With Ages and Durations According to Different Published Geomagnetic Polarity Timescales

Pol. Chron	Depth of Base of pol. zone (mcd)	Onset/Duration (kyr) [*Billups et al.*, 2004]	Onset/Duration (kyr) [*Pälike et al.*, 2006]	Onset/Duration (kyr) [*Lourens et al.*, 2004; *Ogg and Smith*, 2004]
C1n	0.75			781 / 781
C1r.1r	1.92			988 / 84
C1r.1n	2.08			1072 / 101
C1r.3r	2.75			1778 / 593
C2n	3.16			1945 / 167
C3n.4n	4.08			5235 / 798
C3r	5.33			6033 / 219
C3An.2n	6.33			6733 / 297
C3Br.3r	7.66			7528 / 39
C4n.2n	8.75			8108 / 413
C4r.2r	10.25			8769 / 469
C4An	11.00			9098 / 329
C5n.1r	12.16			9987 / 53
C5n.2n	14.33			11,040 / 1053
C5r.3r	16.75			12,014 / 400
C5An.2n	18.91			12,415 / 208
C5Ar.3r	21.66			13,015 / 137
C5AAn	22.25			13,183 / 168
C5AAr	23.08			13,369 / 186
C5ABn	24.75			13,605 / 236
C5ABr	25.42			13,734 / 129
C5ACn	26.81			14,095 / 361
C5ACr	27.22			14,581 / 387
C5ADn	28.60			14,194 / 99
C5ADr	29.58			14,784 / 203
C5Bn.1n	29.90			14,877 / 93
C5Bn.1r	30.76			15,032 / 155
C5Bn.2n	31.53	15,160	15,160	15,160 / 128
C5Br	36.66	15,898 / 738	15,899 / 739	15,974 / 814
C5Cn.1n	38.19	16,161 / 263	16,162 / 263	16,268 / 294
C5Cn.1r	38.61	16,255 / 94	16,256 / 94	16,303 / 35
C5Cn.2n	38.88	16,318 / 63	16,319 / 63	16,472 / 169
C5Cn.2r	39.30	16,405 / 87	16,406 / 87	16,543 / 71
C5Cn.3n	39.72	16,498 / 93	16,499 / 93	16,721 /178
C5Cr	41.80	17,003 / 505	17,004 / 505	17,235 / 514
C5Dn	42.84	17,327 / 324	17328 / 324	17,533 / 298
C5Dr.1r	43.60	17,511 / 184	17,512 / 184	17,717 / 184
C5Dr.1n	43.83	17,550 / 39	17,551 / 39	17,740 / 23
C5Dr.2r	44.86	17,948 / 398	17,948 / 397	18,056 / 316
C5En	47.08	18,431 / 483	18,432 / 484	18,524 / 468
C5Er	48.19	18,614 / 183	18,616 / 184	18,748 / 224
C6n	58.05	19,599 / 985	19,599 / 983	19,722 / 974
C6r	61.81	19,908 / 309	20,001 / 402	20,040 / 318
C6An.1n	63.47	20,185 / 277	20,227 / 226	20,213 / 173
C6An.1r	65.42	20,420 / 235	20,425 / 198	20,439 / 226
C6An	68.54	20,720 / 300	20,652 / 227	20,709 / 270
C6Ar	73.68	21,150 / 430	21,114 / 462	21,083 / 374
C6AAn	75.07	21,191 / 41	21,197 / 83	21,159 / 76
C6AAr.1r	79.93	21,457 / 266	21,507 / 310	21,403 / 244
C6AAr.1n	81.53	21,542 / 85	21,636 / 129	21,483 / 80
C6AAr.2r	85.35	21,737 / 195	21,743 / 107	21,659 / 176
C6AAr.2n	85.97	21,780 / 43	21,780 / 37	21,688 / 29
C6AAr.3r	86.94	21,847 / 67	21,853 / 73	21,767 / 79
C6Bn.1n	89.17	21,991 / 144	21,998 / 145	21,936 / 169
C6Bn.1r	89.79	22,034 / 43	22,062 / 64	21,992 / 56
C6Bn.2n	94.72	22,291 / 257	22,299 / 237	22,268 / 276
C6Br	98.26	22,593 / 302	22,588 / 289	22,564 / 296
C6Cn.1n	100.00	22,772 / 179	22,685 / 97	22,754 / 190
C6Cn.1r	102.50	22,931 / 159	22,854 / 169	22,902 / 148

Table 1. (continued)

Pol. Chron	Depth of Base of pol. zone (mcd)	Onset/Duration (kyr) [*Billups et al.*, 2004]	Onset/Duration (kyr) [*Pälike et al.*, 2006]	Onset/Duration (kyr) [*Lourens et al.*, 2004; *Ogg and Smith*, 2004]
C6Cn.2n	103.96	23,033 / 102	23,026 / 172	23,030 / 128
C6Cn.2r	107.50	23,237 / 204	23,278 / 252	23,249 / 219
C6Cn.3n	108.68	23,299 / 62	23,340 / 62	23,375 / 125
C6Cr	119.10	23,988 / 689	24,022 / 682	24,044 / 670
C7n.1n	119.58	24,013 / 25	24,062 / 40	24,102 / 57
C7n.1r	120.76	24,138 / 125	24,147 / 85	24,163 / 61
C7n.2n	125.63			24,556 / 393
C7r	130.49			24,915 / 359
C7An	132.50			25,091 / 175
C7Ar	135.07			25,295 / 204
C8n.1n	137.71			25,444 / 149
C8n.1r	138.33			25,492 / 48

Magnetite is clearly the dominant magnetic mineral in these sediments.

[17] Plots of anhysteretic susceptibility versus susceptibility, using the empirical magnetite grain size calibration from *King et al*. [1983], implies magnetite grain sizes predominantly <0.1 μm at both Site U1334 and Site U1335 (Figure 9). Hysteresis ratios plotted on a Day plot (Figure 10a) lie within the PSD field and in the finer-grained part of the SD to MD magnetite grain-size mixing line [*Carter-Stiglitz et al*., 2001; *Dunlop and Carter-Stiglitz*, 2006; *Dunlop*, 2002a, 2002b] that corresponds to magnetite grain sizes less than 0.1 μm according to an empirical calibration using sized (unannealed) titanomagnetite [*Dunlop*, 2002a].

[18] FORC diagrams at both sites are characterized by well-defined ridges elongated along the H_c axis with little spread along the H_u axis (Figure 10b).

Table 2. Depths of Onset of Polarity Chrons Recorded at Site U1335, With Ages and Durations According to Different Published Geomagnetic Polarity Timescales

Pol. Chron	Depth of Base of pol. Zone (mcd)	Onset / Duration (kyr) [*Billups et al.*, 2004]	Onset / Duration (kyr) [*Pälike et al.*, 2006]	Onset / Duration (kyr) [*Lourens et al.*, 2004; *Ogg and Smith*, 2004]
C5AAn	125.00			13,183 / 168
C5AAr	128.60			13,369 / 186
C5ABn	131.50			13,605 / 236
C5ABr	136.60			13,734 / 129
C5ACn	140.65			14,095 / 361
C5ACr.1r	142.27			14,134[1] / 39[1]
C5ACr.1n	142.77			14,146[1] / 12[1]
C5ACr.2r	144.72			14,194 / 47[1]
C5ADn	154.79			14,581 / 387
C5ADr	155.76			14,784 / 203
C5Bn.1n	157.34			14,877 / 93
C5Bn.1r	162.34			15,032 / 155
C5Bn.2n	168.30			15,160 / 128
C5Br	184.35	15,898 / 738	15,899 / 739	15,974 / 814
C5Cn.1n	189.55	16,161 / 263	16,162 / 263	16,268 / 294
C5Cn.1r	191.06	16,255 / 94	16,256 / 94	16,303 / 35
C5Cn.2n	191.90	16,318 / 63	16,319 / 63	16,472 / 169
C5Cn.2r	193.30	16,405 / 87	16,406 / 87	16,543 / 71
C5Cn.3n	194.35	16,498 / 93	16,499 / 93	16,721 / 178
C5Cr	201.90	17,003 / 505	17,004 / 505	17,235 / 514
C5Dn	207.00	17,327 / 324	17,328 / 324	17,533 / 298
C5Dr.1r	210.00	17,511 / 184	17,512 / 184	17,717 / 184
C5Dr.1n	210.66	17,550 / 39	17,551 / 39	17,740 / 23
C5Dr.2r	216.50	17,948 / 398	17,948 / 397	18,056 / 316
C5En	225.92	18,431 / 483	18,432 / 484	18,524 / 468

[1]Estimated from Site U1335.

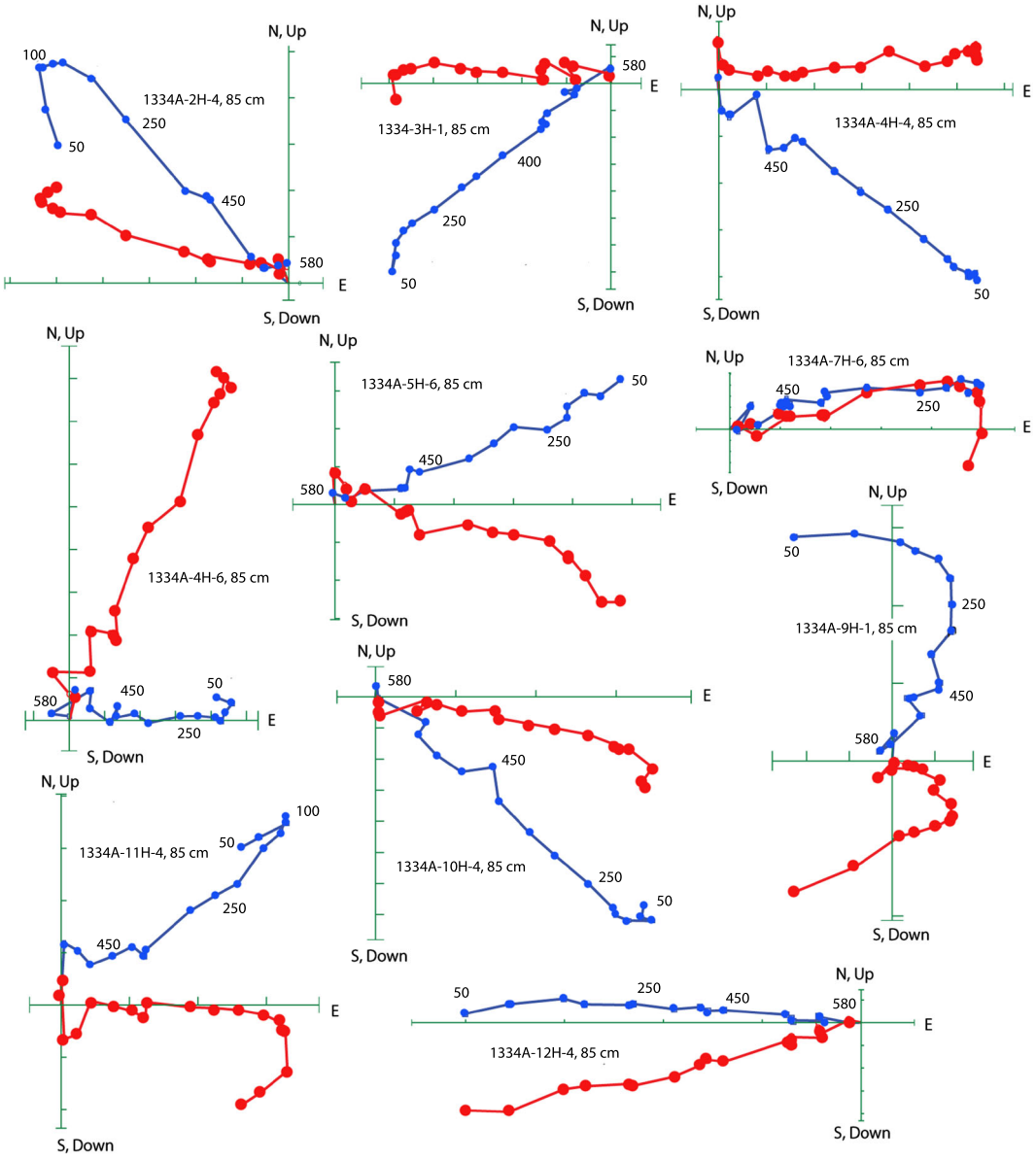

Figure 7. Site U1334: Orthogonal projections of thermal demagnetization data in the 50–580°C interval. Red and blue symbols represent projections onto the vertical and horizontal planes, respectively. Scale: one division is equivalent to 10^{-4} A/m. Temperatures associated with certain points are indicated in degrees Celsius. Declinations are relative to the split face of core sections.

The well-defined ridge aligned with the H_c axis, combined with a concentration of coercivities centered at ~30 mT (Figure 10b), is reminiscent of FORC diagrams that have recently been documented in sediments from the equatorial and southern Pacific and the southern Indian oceans [*Roberts et al.*, 2011, 2012; *Yamazaki*, 2012; *Yamazaki and Ikehara*, 2012; *Larrasoaña et al.*, 2012]. We interpret the FORC diagrams (Figure 10b) as being characteristic of a magnetite population dominated by dispersed (unclumped) biogenic (bacterial) magnetite, possibly with some intact magnetosome chains [see *Egli et al.*, 2010].

5. Transmission Electron Microscopy

[19] Magnetic extracts for electron microscopy were made from sediments scraped off the sides of u-channels during sampling of Core U1335B-21H. Sediment was reacted with Na acetate buffered glacial acetic acid (pH = 5) for over 12 h, centrifuged

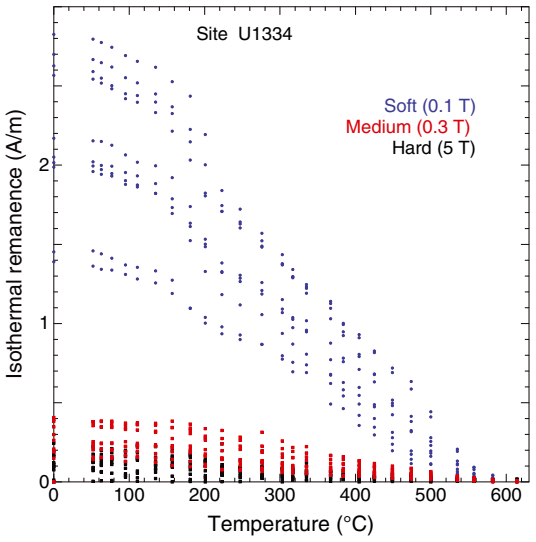

Figure 8. Thermal demagnetization of a 3-axis IRM applied orthogonally and sequentially in DC fields of 5 T (black), 0.3 T (red), and 0.1 T (blue).

to separate the liquid, and then treated again with the buffered acetic acid. The carbonate-free sediment was then sonicated in a sodium metaphosphate solution to disperse the grains. The dispersed sediment slurry was then placed in an apparatus where a peristaltic pump drives the fluid slowly, without turbulence, past the outside of a test-tube containing a rare earth magnet. The material adhered to the outside of the test-tube was then removed with a methanol solution. A 3 mm Type-B copper transmission electron microscopy (TEM) grid was floated on the methanol solution with a rare earth magnet, located in a test-tube, suspended over the solution to attract magnetic particles from the methanol solution to the grid. The grid was then picked, with vacuum tweezers, from the methanol surface as the magnet was simultaneously removed. A JEOL JEM-2010 F high-resolution transmission electron microscope was used for imaging and energy dispersive X-ray spectroscopy at an accelerating voltage of 200 kV. The microscope is equipped with a Gatan MultiScan Camera Model 794 for imaging and an Oxford Instruments detector with INCA 4.05 software for microanalysis. Spot analysis and line-scans were conducted in STEM mode with a nominally ~1 nm probe size and a camera length of 12 cm.

[20] Euhedral grains, generally smaller than 100 nm across, but occasionally reaching 200 nm, were observed on the TEM grid (Figure 11). Energy dispersive X-ray spectroscopy data from spot sampling (Figure 11) and line scans (Figure 12) indicate that these grains contain Fe, O but no detectable Ti. In view of the magnetic evidence for ultrafine magnetite, we interpret these imaged grains as magnetite. The size and shape of particles, and absence of Ti, are consistent with these grains having been produced by magnetotactic bacteria [see *Kopp and Kirschvink*, 2008; *Roberts et al*., 2011, 2012; *Yamazaki*, 2012; *Yamazaki and Ikehara*, 2012; *Larrasoaña et al*., 2012; *Chang et al*., 2012]. Detrital magnetite does not, in general, have the size, shape, and compositional characteristics of the grains observed here.

6. Discussion

[21] At Site U1334, apart from the 2–5 Ma interval (the entire Pliocene), the polarity stratigraphy is interpretable from surface sediment back into the Late

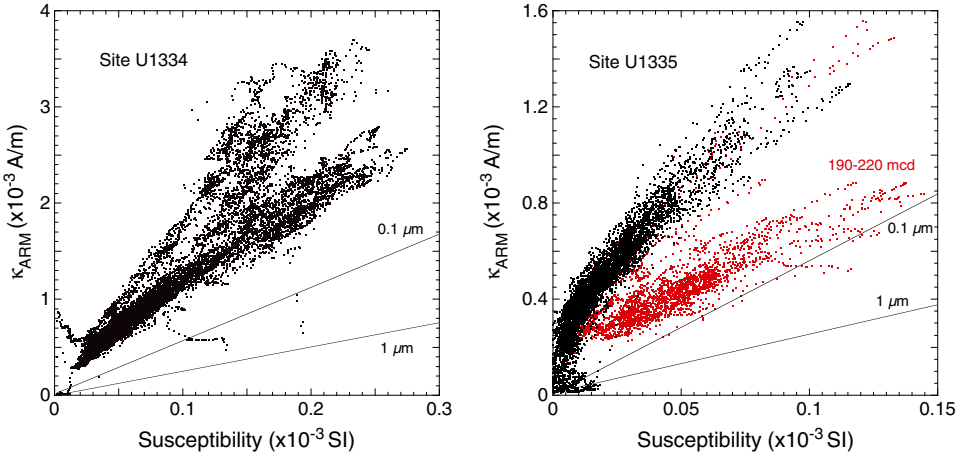

Figure 9. Plot of anhysteretic susceptibility (κ_{ARM}) against susceptibility (κ) with the calibration of magnetite grain size from *King et al*. [1983]. Red symbols for Site U1335 are data from the 190–220 mcd interval.

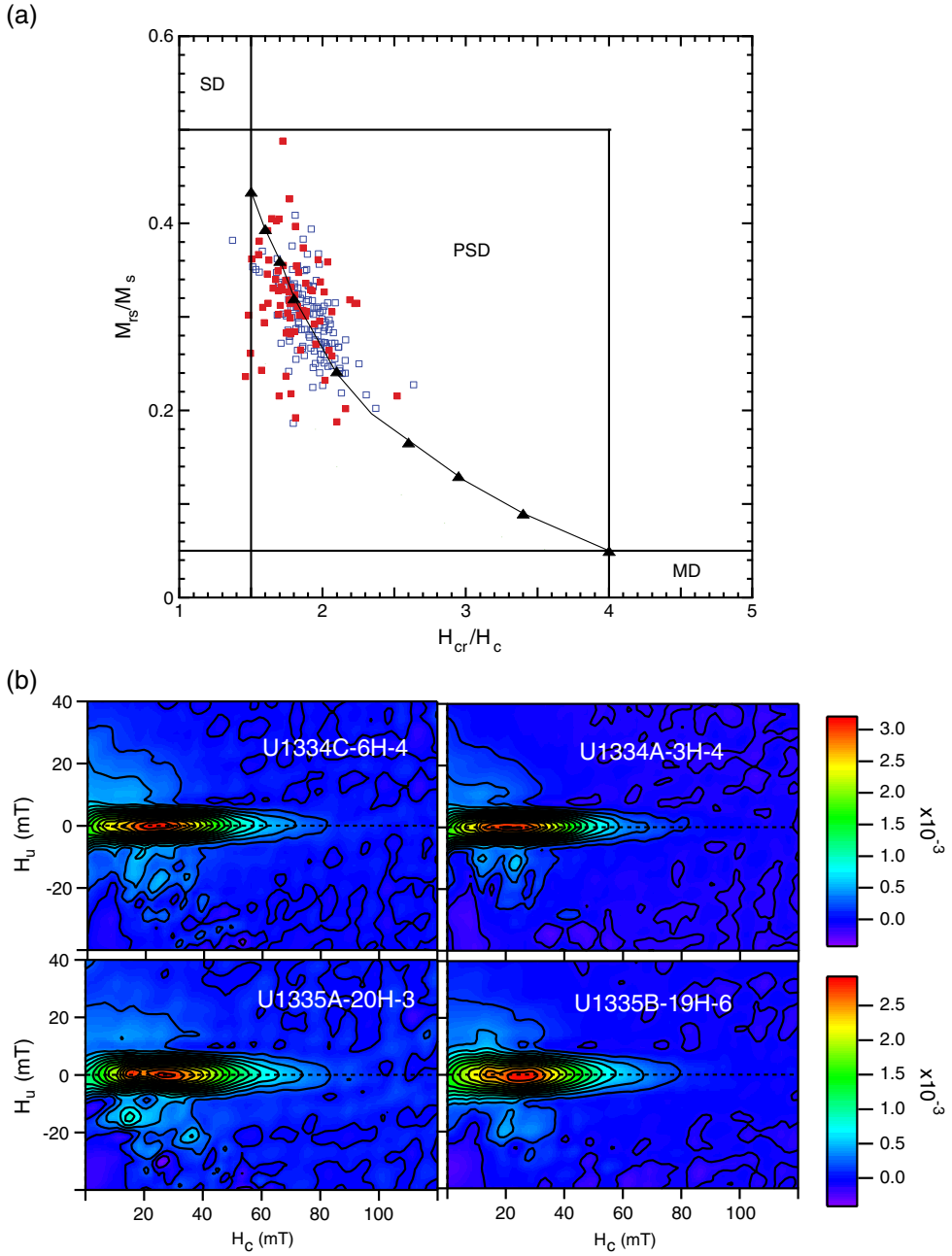

Figure 10. (a) Hysteresis ratio plot after *Day et al*. [1977] for samples Site U1334 (blue open squares) and U1335 (red closed squares) lying along a magnetite grain size mixing line (black closed triangles: *Carter-Stiglitz et al*. [2001]; *Dunlop and Carter-Stiglitz* [2006]; *Dunlop* [2002a, 2002b]) in the PSD field between SD and MD end members. (b) FORC diagrams for sites U1334 and U1335. FORC diagrams were constructed using smoothing factor = 6, and the FORCinel software of *Harrison and Feinberg* [2008].

Oligocene (Chron C8r) at ~26.5 Ma (Figures 3 and 4, Table 1). Sedimentation rates were less than 5 m/Myr for the last 12 Ma and reached 20 m/Myr in the Early Miocene and late Oligocene (Figure 6a). Below 155 mcd (Chron C8r, ~26.5 Myr), the color change from tan-white sediments above, to gray-green sediments below, corresponds to an abrupt decrease in remanence intensities and susceptibility values (Figure 2a). This close correspondence between sediment color and magnetic properties is the rule at sites U1335 and U1334, and determines the feasibility of resolving a magnetic polarity stratigraphy.

[22] At Sites U1334 and U1335, higher magnetization intensities and susceptibility values are closely

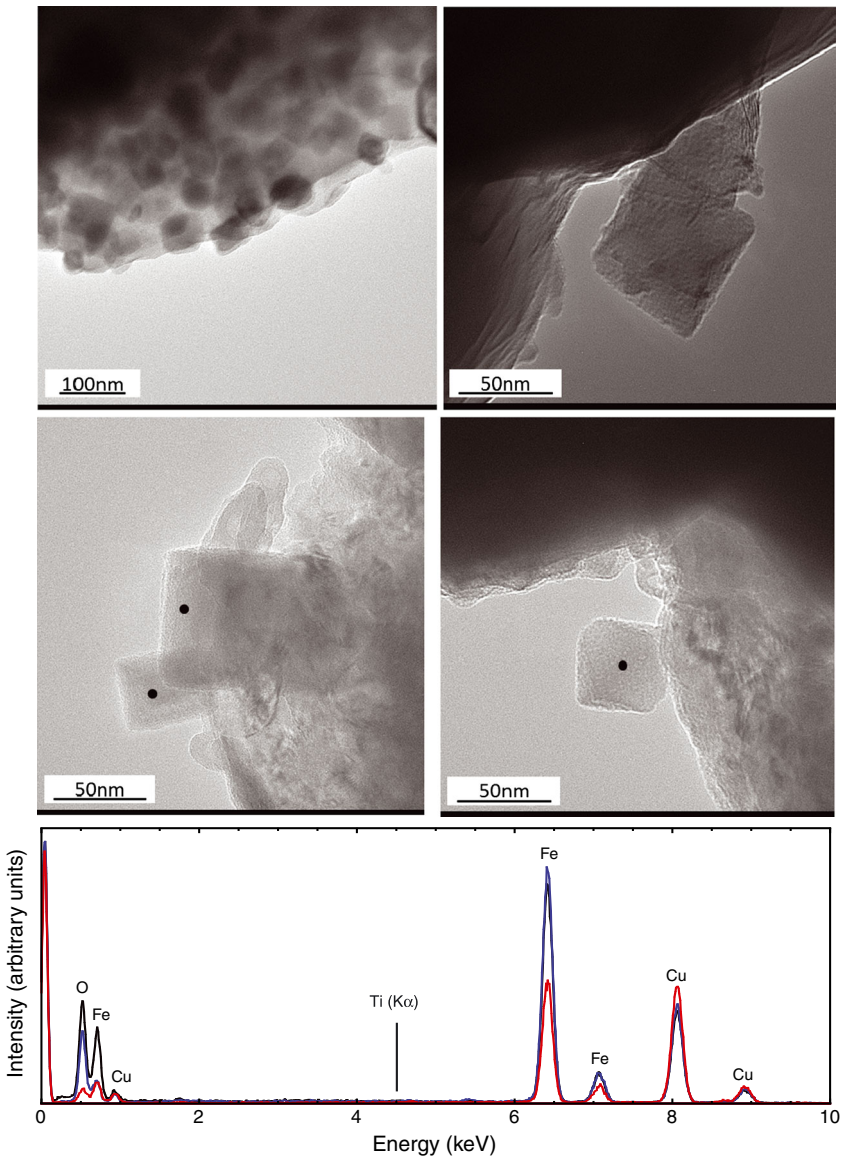

Figure 11. TEM micrographs of particles with a size and shape that are consistent with the presence of biogenic magnetite. Energy dispersive X-ray spectra indicate Fe, O, and Cu (from grid), but no detectable Ti.

tied to sediment color, exemplified by a* (green-red) reflectance (see *Expedition 320/321 Scientists* [2010a, 2010b], Figures F32 and F26, respectively). The greenish sediments have low susceptibility and weak remanence intensities (e.g., the transition at 155 mcd at Site U1334 in Figure 2a). Pore-water sulfate at sites U1334 and U1335 has concentrations close to seawater values (>22 mM) throughout the sedimentary section for which data are available, down to ~450 mcd and ~300 mcd, respectively [*Expedition 320/321 Scientists*, 2010a, 2010b], implying low levels of diagenetic sulfate reduction. Low levels of sulfate reduction can be attributed to low rates of labile organic-matter burial that arrested the activity of sulfate-reducing microbes. At sites U1334 and U1335, total organic carbon in surface sediment is only ~0.15 wt% with values <0.01 wt% (Site U1334) and <0.05 wt% (Site U1335) below the top few tens of meters of the sediment sequence [*Expedition 320/321 Scientists*, 2010a, 2010b]. Labile organic matter in this region is largely oxidized in the water column and in surface sediment by the activity of benthic organisms, including magnetotactic bacteria. These conditions explain the preservation of bacterial magnetite in certain parts of the sediment sequence. Gray-green sediments at sites U1334

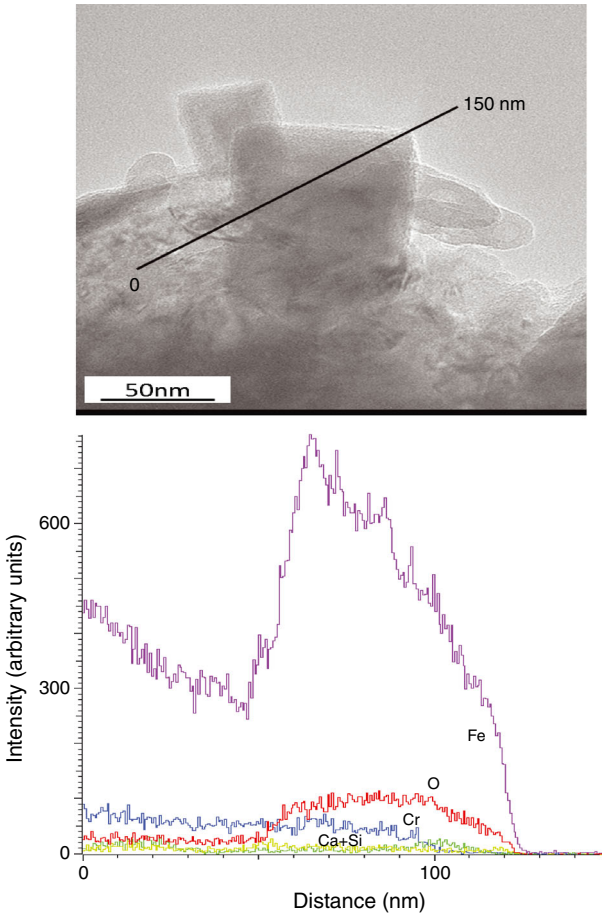

Figure 12. TEM micrograph overlain by a line that indicates the position of an energy dispersive X-ray line-scan, and corresponding intensity versus distance plot.

and U1335, denoted by low values of a* reflectance [*Expedition 320/321 Scientists*, 2010a, 2010b], are largely stripped of their magnetite as a result of marginally higher sedimentation rates and slightly elevated organic matter burial. In the case of Site U1335, and generally for sites U1334 to U1338, zones of marginally higher sedimentation rates coincide with gray-green sediment color (Figure 13). The higher sedimentation rates result in enhanced organic matter burial, and therefore contribute to partial or complete magnetite dissolution.

[23] At Site U1334, sedimentation rates in the 16–17 Ma interval are more variable using the *Lourens et al*. [2004] GPTS than for the *Billups et al*. [2004] GPTS, at both Site U1334 and Site U1335 (Figure 6). This implies inaccurate durations for polarity chrons in the *Lourens et al*. [2004] GPTS in this interval, particularly for Chron C5Cn.1r. This polarity chron has a duration of 94 kyr according to *Billups et al*. [2004] and *Pälike et al*. [2006], but a duration of 35 kyr in the *Lourens et al*. [2004] GPTS (Table 1). On the other hand, peaks in sedimentation rates at Site U1334 for Chrons C6AAn and C6AAr.2r according to the *Billups et al*. [2004] and *Pälike et al*. [2006] GPTSs, respectively, indicate anomalous polarity chron durations in these two timescales for these two polarity chrons (Figure 6a). For Chron C6AAn, the duration in the *Billups et al*. [2004] GPTS is about half those in the other two GPTSs (Table 1). For C6AAr.2r, the duration in the *Pälike et al*. [2006] GPTS, is about half those in the other two GPTSs (Table 1). We note that the Chron C6AAr.2r recorded at ODP

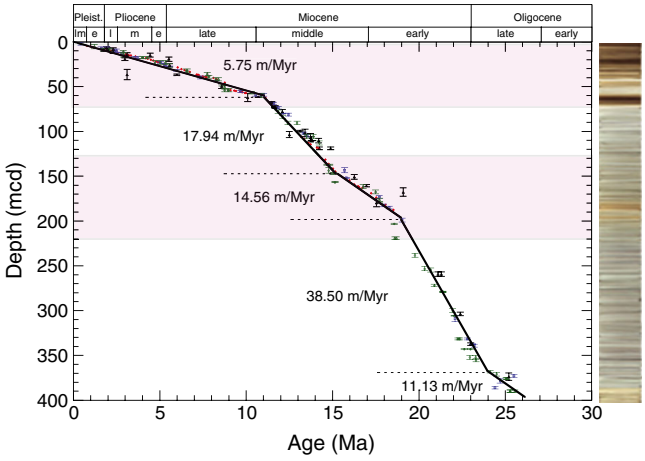

Figure 13. Site U1335 age-depth plot using magnetostratigraphic data (red symbols) and biostratigraphic data (other symbols) (modified after Figure F14 in *Expedition 320/321 Scientists* [2010b]). Shaded areas represent zones of interpretable magnetic polarity stratigraphies, flanked by zones of higher sedimentation rates where magnetite dissolution has occurred.

Site 1218, the basis for the *Pälike et al*. [2006] GPTS, is in an interval where shipboard data had to be used because of a gap in u-channel data [*Lanci et al*., 2004].

[24] At Site U1334, the decrease in sedimentation rate at ~18.5 Ma and subsequent partial recovery in sedimentation rate at 16 Ma (Figure 6a) coincides with the postulated shoaling of the carbonate compensation depth [*Lyle*, 2003], coinciding with independent evidence for increase in atmospheric CO_2 [see *Pälike et al*., 2012]. Site U1335 is not affected by this shoaling of the carbonate compensation depth because of its shallower paleodepth during this (Burdigalian) part of the Miocene.

[25] At Site U1335, sampling and polarity interpretation was limited to a ~104 m interval in the Serravallian to Burdigalian interval of the Miocene. This interval has a more tan-white (rather than green) sediment color, and was chosen because shipboard results indicated the potential to obtain an interpretable magnetic stratigraphy at relatively elevated sedimentation rates (Figure 6). The magnetic polarity interpretation at Site U1335 is considered robust in the 166–227 mcd interval, which corresponds to the Chron C5Bn.2n to C5Er (15.1–18.6 Ma) interval, but is less robust in the 123–166 mcd interval (Figure 5). The magnetic stratigraphy is affected by numerous centimeter- to decimeter-scale beds with sharp basal contacts, which were interpreted shipboard as gravity flow deposits. These redeposited layers are manifested as intervals of weak NRM and ARM intensities (Figure 2b) and poorly defined component magnetizations. Nonetheless, the magnetic stratigraphy at Site U1335 represents a high fidelity record of a problematic interval of the polarity timescale, the Burdigalian to Serravallian (lower-middle Miocene) interval.

[26] Subchron C5Dr.1n is observed at both sites, although it is known from only one other sedimentary record namely ODP Site 1090 in the South Atlantic Ocean [*Channell et al*., 2003]. Chron C5ACr.1n is observed at Site U1335 although it is again only known from one South Atlantic site (ODP Site 1092; *Evans and Channell* [2003]). Putative polarity subchrons, which do not appear in current polarity timescales, occur within Chrons C5ACr, C5ADn, and C5Bn.1r at Site U1335; and within Chrons C6AAr.2r, C6Br, C7Ar, and C8n.1n at Site U1334. They are found in intervals with sedimentation rates higher than ~10 m/Myr (Figure 6), namely ~1 cm/kyr, and are probably present throughout but only recorded where sedimentation rates are elevated. These putative subchrons often have an apparent duration of a few tens of kiloyears (Figures 4 and 5).

7. Conclusions

[27] The dominant magnetic mineral at sites U1334 and U1335 is magnetite, as indicated by thermal and alternating field demagnetization, and magnetic hysteresis measurements. The ratio of ARM intensity to susceptibility, and magnetic hysteresis measurements, including FORC diagrams, indicate that magnetite grain sizes are generally below 0.1 μm. Biogenic (bacterial) magnetite is common in surface marine sediment [e.g., *Vali et al*., 1987] but is not always preserved during diagenesis due to its reactivity (related to its low surface area to volume ratio) with sulfide produced by microbial reduction of pore-water sulfate. Based on TEM observations, Site U1335 contains ultrafine euhedral iron oxides (magnetite) with square cross-sections ~50 nm across that are apparently devoid of Ti. These grains have appropriate grain size, grain shape, and low-Ti content, to be considered as analogs to modern bacterial magnetite [see *Kopp and Kirschvink*, 2008] and are similar to fossil magnetosomes from the Pacific and Indian oceans [*Roberts et al*., 2011, 2012; *Yamazaki*, 2012; *Yamazaki and Ikehara*, 2012; *Larrasoaña et al*., 2012; *Chang et al*., 2012]. The magnetic properties of Oligocene-Miocene sediments in the equatorial Pacific Ocean imply that they are dominated by biogenic (bacterial) magnetite. Bacterial magnetosomes may have had a navigational up/down role in facilitating the location of optimal redox conditions [*Kirschvink*, 1980b]; however, the data from sites U1334 and U1335 imply that magnetotactic bacteria were common at the paleoequator where inclination of the field is obviously an inefficient up/down indicator.

[28] Outside the gray-green colored sediments, the white-tan colored nannofossil oozes at sites U1334 and U1335 record magnetic polarity stratigraphies in the 13–19 Ma (early-middle Miocene) interval at Site U1335 and the 0–26 Ma (late Oligocene to recent) interval at Site U1334. Relatively elevated sedimentation rates, up to ~30 m/Myr (Figure 6) for the 12–26 Ma interval at Site U1334, and for entire record at Site U1335, yield robust polarity stratigraphies for the late Oligocene to middle Miocene. Several polarity subchrons not included in the current GPTS are recognized at sites U1334 and U1335, some of which have been tentatively recognized elsewhere. Apparent abrupt sedimentation rate changes at

both sites imply imprecise age calibration in specific intervals of the particular versions of the GPTS. Finally, the relatively elevated sedimentation rates and the fidelity of magnetostratigraphies at sites U1334 and U1335 will facilitate improved resolution of the astrochronological calibration of the geologic timescale, as well as refinements of equatorial Pacific Ocean paleoceanography, for the late Oligocene to middle Miocene interval.

Acknowledgments

[29] Our research was supported by US National Science Foundation Grant OCE-0960999. We thank P. Rumford at the Texas A&M University (Integrated Ocean Drilling Program) core repository for assistance with sampling, K. Huang at the University of Florida for assistance with laboratory measurements, and A. P. Roberts for a constructive review.

References

Billups, K., H. Pälike, J. E. T. Channell, J. C. Zachos, and N. J. Shackleton (2004), Astronomic calibration of the late Oligocene through early Miocene geomagnetic polarity time scale, *Earth Planet. Sci. Lett.*, *224*, 33–44.

Blakely, R. L. (1974), Geomagnetic reversals and crustal spreading rates during the Miocene, *J. Geophys. Res.*, *79*, 2979–2985.

Cande, S. C., and D. V. Kent (1992), A new geomagnetic polarity timescale for the late Cretaceous and Cenozoic, *J. Geophys. Res.*, *97*, 13917–13951.

Cande, S. C., and D. V. Kent (1995), Revised calibration of the geomagnetic polarity timescale for the Late Cretaceous and Cenozoic, *J. Geophys. Res.*, *100*, 6093–6095.

Carter-Stiglitz, B., B. Moskowitz, and M. Jackson (2001), Unmixing magnetic assemblages and the magnetic behavior of bimodal mixtures, *J. Geophys. Res.*, *106*(26), 397–26, 411.

Chang, L., A. P. Roberts, W. Williams, J. D. Fitz Gerald, J. C. Larrasoana, L. Jovane, and A. R. Muxworthy (2012), Giant magnetofossils and hyperthermal events, *Earth Planet. Sci. Letters*, *351-352*, 258–269.

Channell, J. E. T., S. Galeotti, E. E. Martin, K. Billups, H. Scher, and J. S. Stoner (2003), Eocene to Miocene magnetostratigraphy, biostratigraphy, and chemostratigraphy at ODP Site 1090 (sub-Antarctic South Atlantic), *Geol. Soc. Am. Bull.*, *115*, 607–623.

Day, R., M. Fuller, and V. A. Schmidt (1977), Hysteresis properties of titanomagnetites: grain-size and compositional dependence, *Phys. Earth Planet. Inter.*, *13*, 260–267.

Dunlop, D. J. (2002a), Theory and application of the Day plot (Mrs/Ms versus Hcr/Hc) 1. Theoretical curves and tests using titanomagnetite data, *J. Geophys. Res.*, *107*(B3), 2056, doi:10.1029/2001JB000486.

Dunlop, D. J. (2002b), Theory and application of the Day plot (Mrs/Ms versus Hcr/Hc) 2. Application to data for rocks, sediments, and soils, *J. Geophys. Res.*, *107*(B3), 2057, doi:10.1029/2001JB000487.

Dunlop, D. J., and B. Carter-Stiglitz (2006), Day plots of mixtures of superparamagnetic, single domain, pseudosingle domain, and multidomain magnetites, *J. Geophys. Res.*, *111*, B12S09, doi:10.1029/2006JB004499.

Egli, R., A. P. Chen, M. Winklhofer, K. P. Kodama and C.-S. Horng (2010), Detection of non-interacting single domain particles using first-order reversal curve diagrams, *Geochem. Geophys. Geosyst.*, *11*, Q01Z11, doi:10.1029/2009GC002916.

Evans, H. F., and J. E. T. Channell (2003), Upper Miocene magnetic stratigraphy at ODP site 1092 (sub-Antarctic South Atlantic): recognition of "cryptochrons" in C5n.2n, *Geophys. J. Int.*, *153*, 483–496.

Expedition 320/321 Scientists, Site U1334. In: Pälike, H., Lyle, M., Nishi, H., Lyle, M., Raffi, I., Gamage, K., Klaus, A. and the Expedition 320/321 Scientists (2010a), Proc. IODP, 320/321: Tokyo (Integrated Ocean Drilling Program Management International, Inc.), doi: 10.224/iodp.proc.320321.106.2010.

Expedition 320/321 Scientists, Site U1335. In: Pälike, H., Lyle, M., Nishi, H., Lyle, M., Raffi, I., Gamage, K., Klaus, A. and the Expedition 320/321 Scientists (2010b), Proc. IODP, 320/321: Tokyo (Integrated Ocean Drilling Program Management International, Inc.), doi:10.224/iodp.proc.320321.107.2010.

Guyodo, Y., J. E. T. Channell, and R. Thomas (2002), Deconvolution of u-channel paleomagnetic data near geomagnetic reversals and short events, *Geophys. Res. Lett.*, *29*, 1845, doi:10.1029/2002GL014963.

Harrison, R. J., and J. M. Feinberg (2008), FORCinel: An improved algorithm for calculating first-order reversal curve distributions using locally weighted regression smoothing, *Geochem. Geophys. Geosyst.*, *9*, Q05016, doi:10.1029/2008GC001987.

King, J. W., S. K. Banerjee, and J. Marvin (1983), A new rock-magnetic approach to selecting sediments for geomagnetic paleointensity studies: application to paleointensity for the last 4000 years, *J. Geophys. Res. 88*(1983), 5911–5921.

Kirschvink, J. L. (1980a), The least squares lines and plane analysis of paleomagnetic data, *Geophys. J.R. Astron. Soc. 62*, 699–718.

Kirschvink, J. L. (1980b), South-seeking magnetic bacteria, *J. Exp. Biol.*, *86*, 345–347.

Klitgord, K. D., S. P. Heustis, J. D. Mudie, and R. L. Parker (1975), An analysis of near-bottom magnetic anomalies: sea floor spreading and the magnetized layer, *Geophys. J. R. Astron. Soc. 43*, 387–424.

Kopp, R. E., and J. L. Kirschvink (2008), The identification and biogeochemical interpretation of fossil magnetotactic bacteria, *Earth Sci. Rev.*, *86*, 42–61.

Lanci, L., J. M. Pares, J. E. T. Channell, and D. V. Kent (2004), Miocene magnetostratigraphy from Equatorial Pacific sediments (ODP Site 1218, Leg 199), *Earth Planet. Sci. Lett.*, *226*, 207–224.

Lanci, L., J. M. Pares, J. E. T. Channell, and D. V. Kent (2005), Oligocene magnetostratigraphy from Equatorial Pacific sediments (ODP Sites 1218 and 1219, Leg 199), *Earth Planet. Sci. Lett.*, *237*, 617–634.

Larrasoaña, J. C., A. P. Roberts, L. Chang, S. A. Schellenberg, J. D. Fitz Gerald, R. D. N., and J. C. Zachos (2012), Magnetotactic bacterial response to Antarctic dust supply during the Palaeocene-Eocene thermal maximum, *Earth Planet. Sci. Lett.*, *333-334*, 122–133.

Lourens, L., F. J. Hilgen, N. J. Shackleton, J. Laskar, and D. Wilson (2004), The Neogene Period, in *A Geologic Time Scale*, edited by F. M. Gradstein, J. G. Ogg, and A. G. Smith, pp. 409–440, Cambridge University Press, Oxford, UK.

Lowrie, W. (1990), Identification of ferromagnetic minerals in a rocky by coercivity and unblocking temperature properties, *Geophys. Res. Lett.*, *17*, 159–162.

Lyle, M. (2003), Neogene carbonate burial in the Pacific Ocean, *Paleoceanography*, *18*, 1–21.

Muxworthy, A. R., and A. P. Roberts (2007), First-order reversal curve (FORC) diagrams, in *Geomagnetism and Paleomagnetism*, edited by D. Gubbins and E. Herrero-Bervera, pp. 266–272, Springer, Dordrecht, Netherlands.

Ogg, J. G., and A. G. Smith (2004), The geomagnetic polarity time scale, in *A Geologic Time Scale*, edited by F. M. Gradstein, J. G. Ogg, and A. G. Smith, pp. 63–86, Cambridge University Press, Oxford, UK.

Opdyke, N. D., L. H. Burkle, and A. Todd (1974), The extension of the magnetic time scale in sediments of the Central Pacific Ocean, *Earth Planet. Sci. Lett.*, *22*, 300–306.

Pälike, H., R. D. Norris, J. O. Herrle, P. A. Wilson, H. K. Coxall, C. H. Lear, N. J. Shackleton, A. K. Tripati, and B. S. Wade (2006), The heartbeat of the Oligocene climate system, *Science*, *314*, 1894–1898.

Pälike, H., M. Lyle, M. Nishi, I. Raffi, K. Gamage, A. Klaus and the Expedition 320/321 Scientists (2010), Proc. IODP, 320/321: Tokyo (Integrated Ocean Drilling Program Management International, Inc.), doi:10.224/iodp.proc.320321.

Pälike, H., et al. (2012), A Cenozoic record of the equatorial Pacific carbonate compensation depth, *Nature 488*, 609–614, doi:10.1038/nature11360.

Pares, J. M., and L. Lanci (2004), A Middle Eocene – Early Eocene magnetic polarity stratigraphy in equatorial Pacific sediments, in *Timescales of the Paleomagnetic Field*, edited by J. E. T. Channell, D. V. Kent, W. Lowrie, and J. G. Meert, pp. 131–140, American Geophysical Union, Washington DC.

Pike, C. R., A. P. Roberts, and K. L. Verosub (1999), Characterizing interactions in fine magnetic particle systems using first order reversal curves, *J. Appl. Phys.*, *85*, 6660–6667, doi:10.1063/1.370176.

Roberts, A. P., C. R. Pike, and K. L. Verosub (2000), First-order reversal curve diagrams: A new tool for characterizing the magnetic properties of natural smples, *J. Geophys. Res.*, *105*(28), 461–28,475, doi:10.1029/2000JB900326.

Roberts, A. P., F. Florindo, G. Villa, L. Chang, L. Jovane, S. M. Bohaty, J. C. Larrasoana, D. Heslop, J. D. Fitz Gerald (2011), Magnetotactic bacterial abundance in pelagic marine environments is limited by organic carbon flux and availability of dissolved iron, *Earth Planet. Sci. Lett.*, *310*, 441–452.

Roberts, A. P., L. Chang, D. Heslop, F. Florindo and J. C. Larrasoana (2012), Searching for single domain magnetite in the "pseudo-single-domain" sedimentary haystack: Implications of biogenic magnetite preservation for sediment magnetism and relative paleointensity determinations, *J. Geophys. Res.*, *117*, B08104, doi:10.1029/2012JB009412.

Schneider, D. A. (1995), Paleomagnetism of some Ocean Drilling Program Leg 138, sediments: Detailing Miocene Stratigraphy, in *Proc. O.D.P., Sci. Results*, edited by N. Pisias et al., pp. 59–72, Ocean Drilling Program, College Station, TX.

Shackleton, N. J., S. Crowhurst, T. Hagelberg, N. G. Pisias, and D. A. Schneider (1995), A new Late Neogene time scale: Application to Leg 138 sites, in *Proc. O.D.P., Sci. Results*, edited by N. G. Pisias et al., pp. 73–104, Ocean Drilling Program, College Station, TX.

Thomas, R., Y. Guyodo, and J. E. T. Channell (2003), U-channel track for susceptibility measurements, *Geochem. Geophys. Geosyst. (G3)*, *1050*, doi:10.1029/2002GC000454.

Theyer, F., and S. R. Hammond (1974), Cenozoic magnetic time scale in deep sea cores: Completion of the Neogene, *Geology 2*, 487–492.

Vali, H., O. Forster, G. Amarantidis, and N. Petersen (1987), Magnetotactic bacteria and their magnetofossils in sediments, *Earth Planet. Sci. Lett.*, *86*, 389–400.

Weeks, R., C. Laj, L. Endignoux, M. Fuller, A. Roberts, R. Manganne, E. Blanchard, and W. Goree (1993), Improvements in long-core measurement techniques: applications in palaeomagnetism and palaeoceanography, *Geophys. J. Int.*, *114*, 651–662.

Xuan, C. and J. E. T. Channell (2009), UPmag: MATLAB software for viewing and processing u-channel or other pass-through paleomagnetic data, *Geochem. Geophys. Geosyst.*, *10*, Q10Y07, doi:1029/2009GC002584.

Yamazaki, T. (2012), Paleoposition of the intertropical convergence zone in the eastern Pacific inferred from glacial-interglacial changes in terregenous and biogenic magnetic mineral fractions, *Geology*, *40*, 151–154.

Yamazaki, T., and M. Ikehara (2012), Origin of magnetic mineral concentration variation in the Southern ocean, *Paleoceanography*, *27*, PA2206, doi:10.1029/2011PA002271.